JACS JOURNAL OF THE AMERICAN CHEMICAL SOCIETY

Article

Cite This: J. Am. Chem. Soc. 2018, 140, 4018−4027

pubs.acs.org/JACS

Energy Landscapes for the Aggregation of Aβ_{17-42}

Konstantin Röder* and David J. Wales*

Department of Chemistry, University of Cambridge, Lensfield Road, Cambridge, CB2 1EW, United Kingdom

Supporting Information

ABSTRACT: The aggregation of the Aβ peptide (Aβ_{1-42}) to form fibrils is a key feature of Alzheimer's disease. The mechanism is thought to be a nucleation stage followed by an elongation process. The elongation stage involves the consecutive addition of monomers to one end of the growing fibril. The aggregation process proceeds in a stop-and-go fashion and may involve off-pathway aggregates, complicating experimental and computational studies. Here we present exploration of a well-defined region in the free and potential energy landscapes for the Aβ_{17-42} pentamer. We find that the ideal aggregation process agrees with the previously reported dock-lock mechanism. We also analyze a large number of additional stable structures located on the multifunnel energy landscape, which constitute kinetic traps. The key contributors to the formation of such traps are misaligned strong interactions, for example the stacking of F19 and F20, as well as entropic contributions. Our results suggest that folding templates for aggregation are a necessity and that aggregation studies could employ such species to obtain a more detailed description of the process.

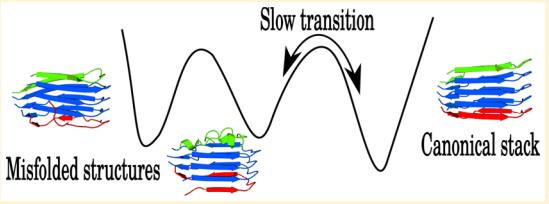

INTRODUCTION

Aggregates of the amyloid-β (Aβ) protein are a key feature of Alzheimer's disease,[1−4] and their formation and properties have been the subject of many studies.[5,6] However, the exact mechanism of pathogenicity is still uncertain, with active research surrounding every aspect of the underlying biochemistry. Aggregates of the 42-residue Aβ peptide (Aβ_{1-42}) lead to the formation of amyloid fibrils, which appear to be a necessary condition for Alzheimer's to develop. Various oligomeric complexes are formed on the pathway to fibrils. It is thought that there are three key processes in fibril formation, namely, primary and secondary nucleation, which both result in the formation of protofibrils that subsequently grow by an elongation process.[7,8] Experimental studies have shown that after an initial phase of primary nucleation, secondary nucleation becomes the dominant protofibril formation process.[9,10] Secondary nucleation in this context refers to the formation of new fibrils on the surface of pre-existing fibrils. It has been found that there are a number of pathways to fibrils via primary aggregation, as well as off-pathway aggregation processes, leading to kinetically trapped oligomeric structures.[11−14] Hence we need to understand the structural ensembles the oligomers and fibrils inhabit, the pathways connecting oligomers to fibrils, and the formation of off-pathway oligomers.

Recently, significant progress has been made in the determination of the peptide structure within Aβ_{1-42} fibrils.[15−20] The elongation process has also been studied extensively, and experiment indicates that aggregation occurs predominantly via the addition of monomers[21,22] with a preferred growth direction.[23] A dock−lock process was proposed, with a reversible docking step followed by an irreversible locking of the monomer to one end of the growing fibril.[21,22] Many further studies support this picture of fibril elongation,[24−40] adding detail. The locking phase has been studied extensively.[30,31,33] It allows for the correct locking outcome as well as non-native locking products, matching the experimentally observed[41−43] "stop-and-go" fibril elongation,[39] with at least two distinct mechanisms for locking.[28,32,33] Recent computational work[34,37,40,44] uses rigid templates and a shortened N-terminus region for simulations of aggregation, and drives the simulation with biased potentials. Alternatively, the molecular dynamics (MD) approach of Bacci et al.[45] constructs a Markov state model for aggregation. The results indicate that the N-terminus region shields the lateral interfaces of the growing fibril. In addition, it was hypothesized that the growing ends of the fibril are disordered and that locking happens progressively at the disordered ends of the aggregate as the rate-limiting step.

Elongation of the strand is theoretically possible at both ends, termed odd and even according to the numbering of the amino acids involved in binding the next strand. We use this nomenclature throughout and in graphical representations, with the odd end colored green and the even end colored red. The fibril elongation is thought to be unidirectional, and many studies have focused on this aspect. Han and Schulten[36] suggest that fibril growth is based on the exposure of residues 17−21 at one end of the strand. A recent study[46] employed MD simulations to study the unidirectional fibril elongation, observing a clear preference for the even end, due to stronger hydrogen bonds and smaller structural fluctuations.

Another all-atom MD study investigated the secondary nucleation on a fibril formed of Aβ_{9-40} fragments[44,47] and observed a β-fibril-like assembly for the trimeric and tetrameric oligomers. The growth of fibrils from these aggregates is

Received: December 9, 2017
Published: February 27, 2018

DOI: 10.1021/jacs.7b12896
J. Am. Chem. Soc. 2018, 140, 4018−4027

probably similar to fibril elongation. Furthermore, this model explains the observation that secondary nucleation is faster than primary nucleation, as the slow global rearrangements required to form protofibrils[48] from oligomeric structures are no longer required. Secondary nucleation, after an initial oligomer is formed on the fibril surface, seems to proceed rapidly to the elongation phase compared to the primary nucleation process.

Various open questions remain, mainly related to the primary nucleation process, as well as to the structural variety of oligomeric Aβ assemblies. As the time scales for aggregation may be difficult to characterize in experiments,[48] there are significant challenges in describing such processes. Furthermore, the oligomers can be short-lived and exhibit significant conformational variety, which leads to additional complications in studying the pathways to fibril formation. There may be many off-pathway aggregates acting as kinetic traps and complicating the process. Here we define a kinetic trap as a region of the energy landscape that the system cannot easily escape from, due to surrounding high energy barriers. More specifically, in the present context a kinetic trap is an off-pathway region of the energy landscape corresponding to noncanonical structures, from which escape is slow. As oligomers are likely candidates for the neurotoxic agents in Alzheimer's disease,[49−51] the increased lifetime of such structures may increase the potential for neurological damage. Characterization of the aggregates is therefore important in understanding the disease better, as well as suggesting new therapeutic strategies.

One of the factors influencing the structural polymorphism of Aβ_{1-42} is the intrinsically disordered nature of the peptide,[52] corresponding to a frustrated energy landscape[53−55] with a large number of low-lying minima exhibiting different structural motifs but separated by high barriers. High barriers for transitions between distinct conformations can lead to broken ergodicity in simulations. These features are the likely origin of the difficulties experienced in experimental and computational studies. Indeed this picture is supported by recent work[56] using MD simulations to study the aggregation free energy landscape for Aβ_{40} and Aβ_{42}. Not surprisingly, biased simulations tend to produce canonically stacked fibril-like structures for oligomers, while unbiased simulations lead to a variety of structures.

In the present work, we apply the computational potential energy landscape framework to study a well-defined set of configurations. We focus on the locking step of the aggregation process and study the resulting oligomers in detail, as well as the pathways between them. We explore the energy landscape using geometry optimization based techniques, which provide access to all the time scales of interest, allowing us to overcome high energy barriers, without constraints on the β-sheet template. The system we consider in detail is the pentamer, which is large enough to support β-sheets, but at the same time computationally tractable for all-atom simulations. To analyze specific features of the pentamer, we have also studied the potential energy landscapes for a monomer and a tetramer. We report a detailed description of possible kinetic traps for the aggregation process and consider the implications for studies of protein aggregation in general.

METHODS

Starting Points and Force Field. All our calculations employed the AMBER[57−59] ff14SB force field,[60] which was properly symmetrized in the same way[61,62] as the ff99SB[63] force field, in combination with an implicit generalized Born solvation model (igb = 2)[64,65] using infinite interaction cutoffs and the Debye−Hückel approximation for salt (0.1 M).[66] The exploration of the monomer energy landscape was initialized from low-energy structures located using basin-hopping[67−69] global optimization using the GMIN program.[70] All Aβ peptides were truncated to residues 17−42, as in the initial structure for the ordered pentamer taken from Protein Databank entry 2BEG.[71] This truncation is useful for computational reasons, as it reduces the computational cost significantly, and the consequences have been studied by Bacci et al.,[45] providing a useful reference for the present work. The initial set of disordered structures was created by restraining the four protein strands at the bottom or top of the stack and heating the structures in molecular dynamics (MD) simulations up to 650 K. Heating was followed by a short 10 ns MD run using a 2 fs time step, SHAKE constraints,[72] and a Langevin thermostat[73] employing a collision frequency of 0.2 ps^{-1}. Selected configurations were minimized using the customized L-BFGS approach in our GMIN[70] and OPTIM[74] programs. Initial tetramer structures were derived from configurations corresponding to the kinetic traps of the pentamer by removing one strand. Additional minima for the pentamer landscape were added by docking tetrameric and monomeric conformations using PyMOL.[75]

Exploration of the Energy Landscapes. Discrete path sampling[76,77] was employed to construct kinetic transition networks,[78,79] consisting of local minima and the transition states that connect them. The doubly-nudged[80] elastic band[81,82] algorithm and hybrid eigenvector-following[83] were used to locate transition states, with approximate steepest-descent paths to obtain the connected minima. All minimizations used the customized L-BFGS approach[84,85] with an RMS force convergence condition of 10^{-6} kcal mol^{-1}. GPU acceleration[86,87] was used to speed up computation via the GPU interface[88] for OPTIM[74] and AMBER12.[59] The initial stationary point databases were expanded using the SHORTCUT[26,89] and UNTRAP[26] schemes within the PATHSAMPLE program,[90] as described in previous work. SHORTCUT identifies alternative pathways to reduce the number of steps in discrete paths and to locate paths avoiding high energy barriers. The UNTRAP scheme is designed to remove artificial kinetic traps by improving the local connectivity between minima. Recent reviews of the methodology employed have been presented by Joseph et al.[91] and Chakraborty and Wales.[92]

To increase the size of the largest connected set in the network, denoted *AB*, and the connectivity of all the other components, a new scheme was employed. First, the minima were separated into two sets, *AB* and $\overline{AB}$. We now either select a minimum *i* within *AB* and find the *n* closest minima in Euclidean distance in $\overline{AB}$ and attempt to find connections between them, or we find the lowest energy minimum in *AB* and find the corresponding *n* closest minima in Euclidean distance in $\overline{AB}$ and attempt these connections. The first option allows us to improve sampling in selected regions of the landscape. Good choices for *i* are low-lying minima in funnels separated from the global minimum and minima in intermediate regions between funnels, which are hard to sample for larger systems. The second option improves the sampling around the global minimum, or in some cases produces a connection between the global minimum and the *AB* set. The procedure is initialized in every cycle of database refinement, alternating between existing schemes. The new algorithm performed very well in sampling the multifunnel and intrinsically disordered landscapes exhibited by the three Aβ systems considered here.

The sampling of the monomer landscape was based on the low-energy structures located by basin-hopping. These structures were connected and the resulting funnels on the landscape further sampled to connect all local structures within the funnel, as well as the pathways between funnels. For the pentamer, alternative databases were initialized corresponding to connections between different ordered and disordered stacks. The databases were then combined, connected, and then further sampling was used to improve the connectivity at the bottom of the funnels and between funnels. For the tetramer landscape, only the local region corresponding to the transition between the in-phase and out-of-phase stacks was sampled. Convergence was tested by analyzing changes in the low temperature heat capacity features, the pathways between funnels, and the overall shape of the landscape, i.e., the appearance of any new features.

DOI: 10.1021/jacs.7b12896
J. Am. Chem. Soc. 2018, 140, 4018−4027

Since the above calculations employ an implicit representation of solvation, we also ran MD simulations for 50 ns in explicit solvent with explicit ions to verify the local stability of the predicted low energy structures under these conditions. All the structures tested were stable on this short MD time scale, with some variability in the docked but unlocked chains. More details are provided in the Supporting Information. The sampling convergence was tested by analyzing the low temperature heat capacity features and visualizing the landscapes using disconnectivity graphs.[93,94] Predicted NMR shifts were calculated using SHIFTX2,[95] and secondary structure assignments are based on DSSP.[96]

RESULTS AND DISCUSSION

$A\beta_{17-42}$ Monomer Energy Landscape. It is well-established that the Aβ peptide in solution is intrinsically disordered.[52] The landscapes associated with intrinsically disordered systems are expected to exhibit multifunnel character with no dominant global minimum, and hence a variety of populated states.[55] The potential energy landscape for the monomer illustrated in Figure 1 clearly fits this pattern. The database contains 70 583 minima and 64 365 transition states, but a large number of high energy minima have not been connected to the set shown in the disconnectivity graph, since they will not affect any of the predicted properties.

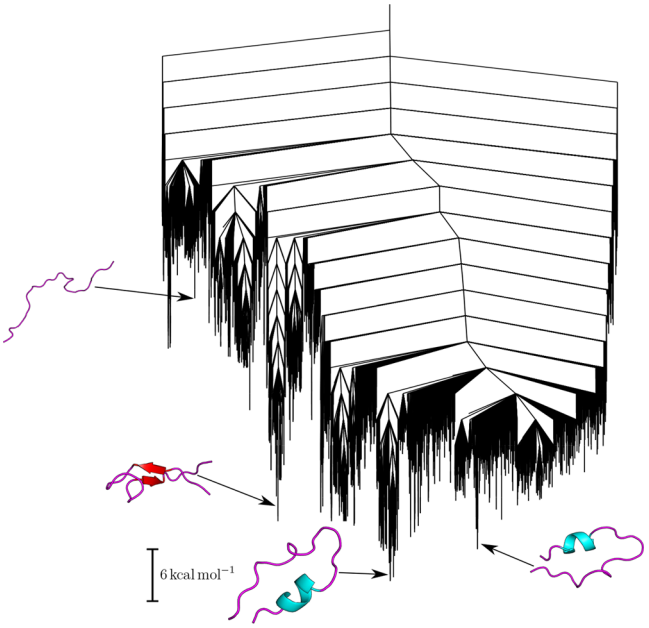

Figure 1. Potential energy landscape for the truncated monomer highlighting the multifunnel character. Many of the low-energy configurations contain helices or lack well-defined secondary structure, but some intramolecular β-sheets are also observed. The structural representations were created using PyMOL.[75]

Our second aim was to find structures that are likely to add to the β-sheet stack to seed the initial exploration of the pentamer landscape via plausible high-energy states, which retain features of the monomeric solution structure when they dock. The low energy conformations are mainly helical or lacking well-defined secondary structure elements, with a small number exhibiting intramolecular β-sheets. These findings agree well with previous studies[52,97] describing the monomeric structures as globular collapsed peptides. Disconnectivity graphs colored to identify the different secondary structure elements are provided in the Supporting Information. Combined MD and NMR studies[98−100] of Aβ monomers have revealed a number of features, which are in good agreement with our results. In particular the characteristic hydrogen bonding for L34/V41 and the stability of salt bridges formed with K28.[99] We observe a preference for D23-K28 salt bridges over E22-K28 salt bridges, which are known to have different biological implications.[101−103] Furthermore, the monomer is described as dynamic, in agreement with the broad range of accessible structures. Additionally, the formation of short helical segments for residues 20−23 and 29−33 has also been observed.[98] Previously reported antiparallel contacts between residues 17−21 and 30−34[100] are also present in a small subset of the structures we have characterized. From these results it is reasonable to conclude that the most likely structures adding to the β-sheet stack resemble the helical or relatively disordered conformations of the monomer, and these were subsequently used to sample the pentamer landscape.

$A\beta_{17-42}$ Pentamer Potential and Free Energy Landscapes. The potential energy landscape, consisting of 48 433 minima and 71 236 transition states, for the $A\beta_{17-42}$ pentamer stack is illustrated in Figure 2. The corresponding free energy surface at 310 K was computed using the harmonic superposition approximation (HSA) to calculate the vibrational contribution to the partition functions,[104] and the resulting free energy disconnectivity graph is shown in Figure 3.

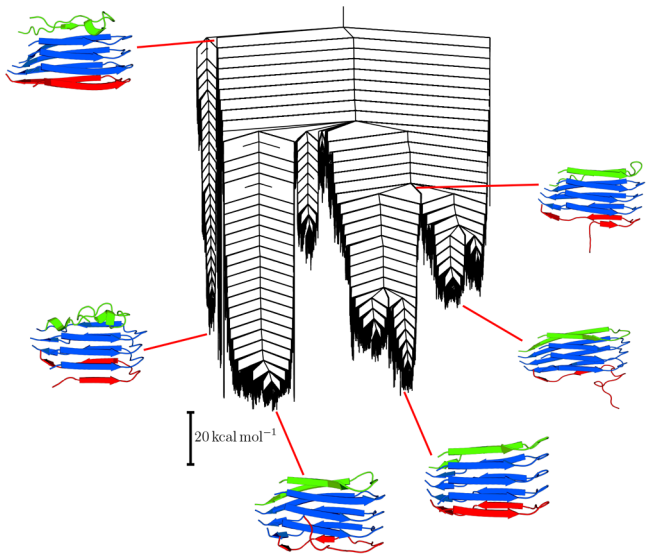

Figure 2. Potential energy landscape for the locking phase, adding a strand to an $A\beta_{17-42}$ tetrameric β-stack, illustrating the canonical assembly as well as kinetic trapping. The structural representations were created using PyMOL.[75]

For both the potential and the free energy landscapes, a number of properties are apparent that confirm the complex picture of the aggregation process developed in previous studies. The energy landscapes exhibit multiple funnels, with large barriers between them, some around 100 kcal mol^{-1}. The resulting slow kinetics and the structural heterogeneity, i.e., the absence of a dominant global minimum energy conformation, agree with the experimentally observed heterogeneity, and clearly explain why enhanced sampling methods, such as bias forces along reaction coordinates, are required for MD simulations.

The large number of funnels separated by high barriers has two immediate effects, namely, fast aggregation of consecutive

DOI: 10.1021/jacs.7b12896
J. Am. Chem. Soc. 2018, 140, 4018−4027

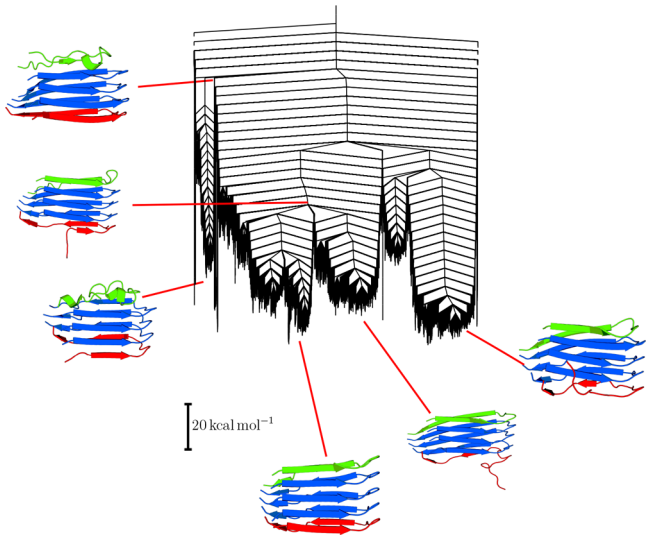

Figure 3. Free energy landscape for the locking phase, adding a strand to an Aβ_{17-42} tetrameric β-stack, illustrating the canonical assembly as well as kinetic trapping. This figure corresponds to the potential energy disconnectivity graph shown in Figure 2.

monomers in an ideal fashion, while the addition of a misaligned monomer requires rearrangements before aggregation can proceed, resulting in a stop-and-go process, in agreement with previous studies.[39,41−43] The off-pathway oligomers can therefore be viewed as traps corresponding to deep funnels with low escape probabilities. This scenario also implies that the locking step is rate determining. To understand the aggregation process we must characterize the kinetic traps and the predicted signatures in experimental observables. Here we will discuss three distinct kinds of traps: traps due to locking of an out-of-register stack, entropic traps within the locking stage, and traps due to twisting of the stack, leading to misalignment at both the even and odd ends. Example structures are shown in Figure 4.

On the basis of the starting point NMR configuration,[71] a number of structural features for the canonical assembly can be identified, which agree with other studies,[46] namely, the interaction between D23 and K28 and the stacking of F19 and F20. These canonical interactions are found in the correctly stacked conformation. In all other funnels, these interactions will be perturbed by associated structural changes. The general mechanism for the formation of any kinetic trap is based on these perturbations of the canonical bonding and contact pattern for a given amino acid. As all conformational changes that reverse these misaligned interactions require breaking and reforming favorable interactions, either one-by-one or as a collective process, the corresponding energy barriers are necessarily large, and are associated with slow dynamics.

Ideal Locking Mechanism. Before we discuss the details of kinetic traps and their relevance to the aggregation process, a brief consideration of the ideal mechanism, i.e., the fastest pathway leading to the canonical structure, in the absence of traps, will be presented. The structures that exhibit large deviations from the canonical stack, which have not completed the locking process, generally exhibit well-defined order in the C-terminus region, in agreement with previous studies.[28,45] Gurry and Stultz,[37] as well as Han and Schulten,[36] observed intermediate states with a characteristic hairpin and intramolecular hydrogen bonds formed between the two β-sheets in the locking monomer. However, we do not observe such structures, in agreement with Bacci et al.[45] For the unconstrained structural ensembles we obtain for stacking, which allow the β-stack to adjust to the locking, such configurations would introduce strain and twisting. The last stage of the locking process is the alignment of the hydrophilic loop region, as in previous work.[28,34,37]

Out-of-Register Configuration Locked by a Docked Coiled Conformation. The first trapping process we consider is enthalpic in nature. The stack is locked in an off-pathway conformation by a coiled conformation attached to the odd end [see Figure 4b]. The funnel containing the trapped structures appears in both the free energy and potential energy landscapes, separated by approximately the same energy barriers. Hence, entropy plays a minor role in this first type of kinetic trap, where the configurations encountered along the transformation pathway are tightly bound, lacking significant structural flexibility.

The key feature of this trap is a register shift of the strands. In the canonical structures, the β-sheets of one strand (β_1 and β_2) are oriented such that the intermolecular interactions between the β-sheets are parallel to the stacking axis, and the first and last residues of β_1 and β_2 are in a plane perpendicular to this axis. In the off-pathway structure they are shifted by one strand such that the first residue in β_1 lines up with the last residue in β_2 in the strand below (see Figure 4). This shift corresponds to a change in the π-stacking pattern of residues F19 and F20, allowing the strands to perform a shear motion, reducing the distance between β_1 and β_2 (Figure 5).

We see similar changes in other parts of the landscape. However, greater stability can arise from the addition of a configuration lacking well-defined secondary structure locking the off-pathway intermediate. Using a threshold of 16 kcal mol^{-1} to regroup the free energy minima,[105] we can highlight

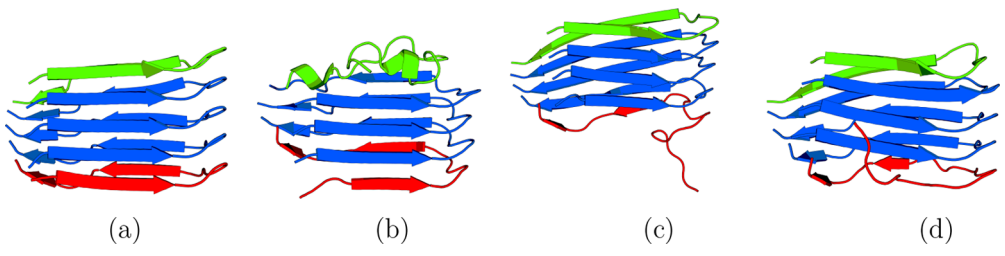

Figure 4. Important structures on the pentamer energy landscape, from left to right: (a) canonical β-stack allowing for continued fibril growth, (b) kinetically trapped configuration due to coiled structure docked to the odd end in an out-of-register stack, (c) kinetically trapped structure that shows a high degree of twisting and disorder at both the odd and even ends, and (d) entropic trap in the free energy landscape due to the large number of possible orientations for the free strand at the even end. All structures were created using PyMOL.[75]

DOI: 10.1021/jacs.7b12896
J. Am. Chem. Soc. 2018, 140, 4018−4027

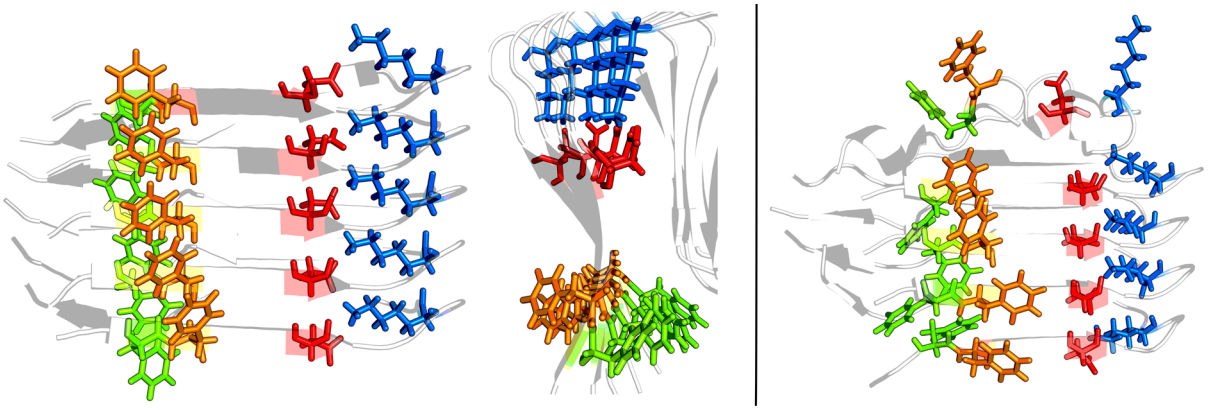

Figure 5. Comparison of the stacking for key residues encountered in the canonical stack (left and middle) with a trapped structure (right). The colored residues are F19 (green), F20 (orange), D23 (red), and K28 (blue). The register shift between the strands corresponds to an alternative stacking of F19 and a change in the F20 stacking compared to the canonical structure. All structures were created using PyMOL.[75]

the principal barriers involved. The free energy profile for the fastest path that results from this analysis is shown in Figure 6. The large barrier height produces a very small computed first order rate constant on the order of 10^{-50} s^{-1}. Hence, this rearrangement process will not be seen at physiological temperatures, and it is likely that dissociation−association would occur instead. In experiments, this process would probably be manifested as stop-and-go aggregation.

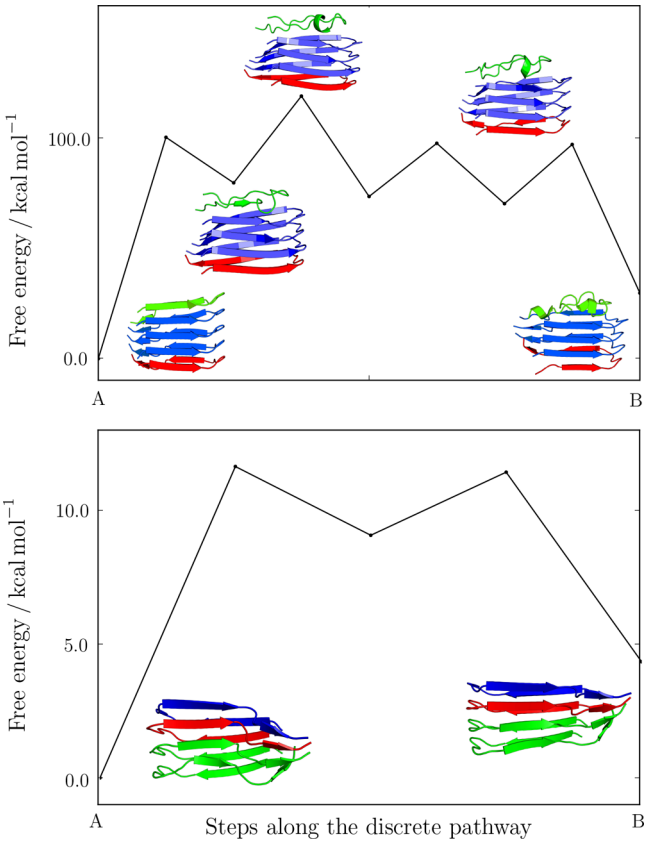

Figure 6. Top: Free energy barriers on the fastest path between the ensemble of structures corresponding to the canonical stack (state A) and the kinetic trapped state (state B). The points correspond to free energy minima and transition states obtained by the recursive regrouping scheme[105] using a barrier threshold of 16 kcal mol^{-1}. Bottom: The same transition for a tetrameric stack reveals a much lower barrier, illustrating the stabilization due to the additional strand in the pentamer. The regrouping threshold was 2.5 kcal mol^{-1}. The steps correspond to regrouped free energy minima and transition states. The structures were created using PyMOL.[75]

In comparison, if we remove the coiled strand from the odd end and probe the transition between the out-of and in-register configurations, then we observe a free energy barrier of less than 10 kcal mol^{-1}, indicating a relatively fast transition, effectively removing the kinetic trap from the landscape. For the tetramer we also encountered a larger number of distortions and twists much lower in energy than the canonical stack. This result agrees with experimental observations that small oligomers do not form β-stacks,[48] unless there is an aggregation template aiding nucleation.[9,10,44] More detail is provided in the Supporting Information.

Misaligned Intermolecular Interactions Lead to Strain and Trapping. It appears that some of the features described above for the first kinetic trap are common to other traps, especially the misalignment of stacking interactions. For the second set of trapped conformations that we have identified (see Figure 4c) we again observe a misalignment in the stacking of F19 and F20, as well as more flexibility in the hydrophilic part of the molecule featuring the salt bridge between K28 and D23 (see Figure 7).

The flexibility in the hydrophilic region is not surprising in aqueous solution, and indeed, it has been observed before[28,34,36] that the hydrophilic region is the last one to lock. The flexibility here certainly allows for a larger accessible configuration space, indicating that disorder is involved in the slow aggregation, in agreement with the recent results of Bacci et al.[45]

This picture is reinforced in analyzing the even end for the trapped configurations, which exhibit an ordered C-terminal region, as seen in other studies,[28,45] but a less ordered arrangement around residues 17−21. The structures are very similar in stability to the canonical stack. Another interesting factor is that this disorder can propagate through the stack, and the closer a strand is to the end, the more variability we observe in the geometry, even though the key structural elements are preserved.

Looking at the differences between higher energy local minima in the transition region between funnels, two features are apparent. First, many higher energy minima exhibit partly detached strands, particularly at the even end, suggesting that

DOI: 10.1021/jacs.7b12896
J. Am. Chem. Soc. 2018, 140, 4018−4027

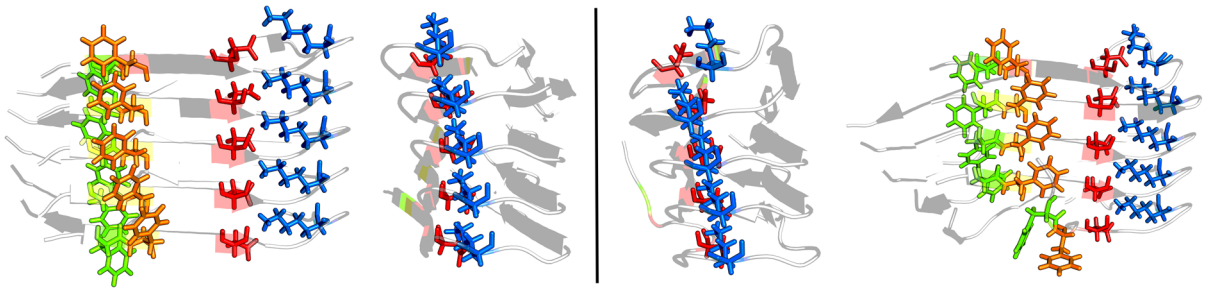

Figure 7. Differences in stacking and alignment between the canonical structure (left) and a misaligned kinetic trap (right). The stacking for F19 and F20 is interrupted, and the loop region of the stack exhibits less order than in the canonical structure. All structures were created using PyMOL.[75]

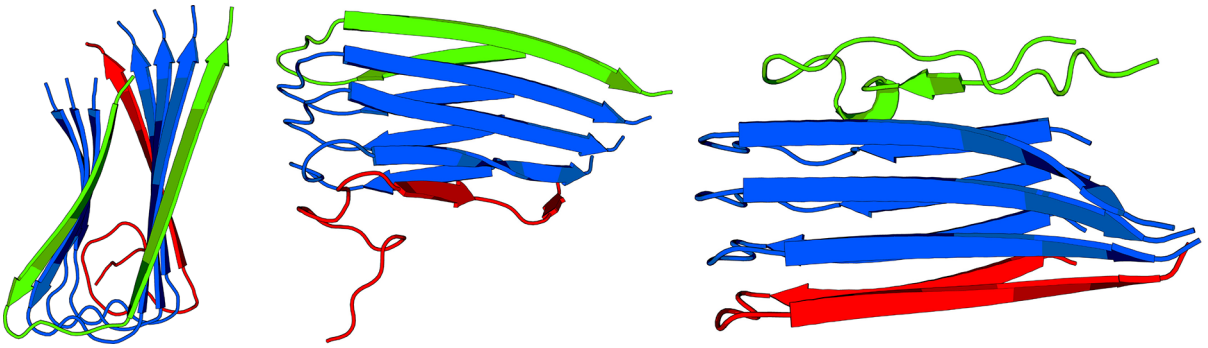

Figure 8. Examples of high-energy structures with strong twisting and partly detached end strands. All structures were created using PyMOL.[75]

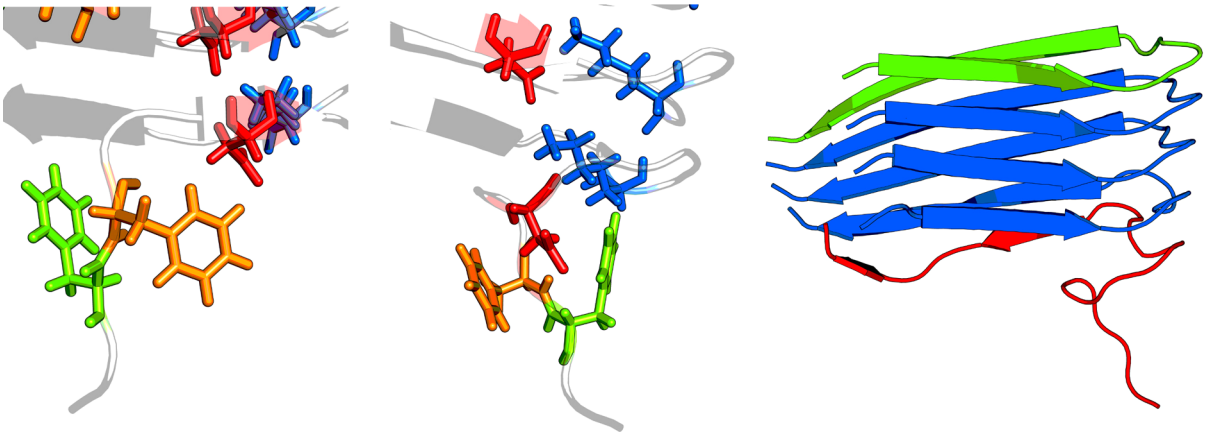

Figure 9. Intramolecular interactions of residues F19, F20, and D23 lead to stabilized high entropy states (left and middle). A full representation of a high entropy configuration reveals the flexibility of residues 17−30, and the fixed C-terminus. All structures were created using PyMOL.[75]

escape from misaligned locked states proceeds via a partial detachment rather than rearrangement in the locked states. The second observation is that longer β-sheets, such as those used in the constrained stack models in previous studies,[34,37] are only encountered in high-energy regions. These longer sheets lead to strain within the stack and twisting. In the lower energy region, the strain is reduced by small deviations from these long β-sheets, particularly in the C-terminal region (Figure 8).

The twisting will be suppressed if structural constraints are applied, such as a biasing potential. It is possible that such constraints produce a structural preference for hairpin structures in other studies, since a canonical β-sheet template may favor these structures. Hairpins may be less likely in unconstrained systems due to the associated strain and twisting in the stack.

Entropy Effects. The kinetic trapping we have considered so far is based mainly on strong but misaligned interactions, stabilizing the noncanonical structures. As a result these traps are apparent in both the potential and the free energy landscapes (see Figures 2 and 3). However, on the free energy landscape additional low-energy states are observed, resulting from entropic contributions to the free energy, which provide another route to kinetic trapping. The common feature of these structures is that they occur at the even end, and the conformational variability that contributes to the entropy is generally associated with residues between 17 and 30. The large number of possible configurations leads to a high entropy state, while at the same time it is possible to form some reasonably strong interactions that stabilize the structures further. Some examples are shown in Figure 9.

Odd and Even End Addition. The observation of kinetic traps agrees with previous studies.[28,34,36,45] In addition, our results provide an interesting perspective on the experimentally observed asymmetric growth of Aβ fibrils. The NMR study by

DOI: 10.1021/jacs.7b12896
J. Am. Chem. Soc. 2018, 140, 4018−4027

Lührs et al. suggested that the odd end grew fastest. However, other studies have arrived at the opposite conclusion.[36,44,46] Bacci et al.[45] find in their simulations that either end can extend, but the inherent asymmetry in the binding sites leads to a preference for the odd end. Our results support this picture, as we observe a larger structural variation in the even end, corresponding to higher entropy. The odd end exhibits smaller fluctuations, indicative of a more tightly bound strand. These effects seem closely related to the binding of residues 17−21, as observed before.[45] The variation in previous studies may be based on how well these effects and their individual contributions have been captured.

NMR Shifts Can Differentiate Funnels on the Energy Landscape. The kinetic traps we have characterized will result in slow dynamics, drastically affecting the ability to study aggregation in experiments. To provide another way of relating our findings to observable properties, we have calculated NMR shifts for the backbone atoms in all the local minima in our pentamer database. In Figure 10, we illustrate the variation of

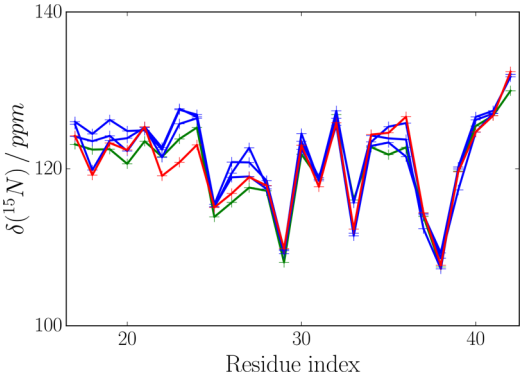

Figure 10. Comparison of the average NMR shifts in ppm for the backbone nitrogen atoms in the five strands of the pentamer. The coloring corresponds to the colors used in the structural representations. The greatest deviation was found for residues 17−27, corresponding to the structural flexibility observed in this region for the oligomers.

the averaged Boltzmann-weighted NMR shifts for the N backbone atoms in the five strands at 298 K. From these chemical shifts, it is apparent that the previously described conservation of structural order in the C-terminus is reproduced, with very small variations observed between the strands. In contrast, the more flexible region of the stack can be identified by larger fluctuations in the average NMR shifts. This structural flexibility is observed for all strands and is still apparent in the core strands, albeit smaller. Furthermore, the shifts observed in the top and bottom strand are close to those calculated for the monomer (see the Supporting Information), confirming the disorder observed in these strands.

These data may also be used to define order parameters and classify regions on the energy landscape. Our first example is illustrated in Figure 11, showing the potential energy disconnectivity graph with a coloring scheme corresponding to the chemical shift for residue F20 of the even end strand. This NMR shift clearly distinguishes distinct regions of the energy landscape, in particular differentiating the canonical stack and the kinetic traps.

The second example is for the out-of-register trap for the odd end. The chemical shift in residue 42 of the odd end strand is clearly different in this trap and the rest of the landscape (see

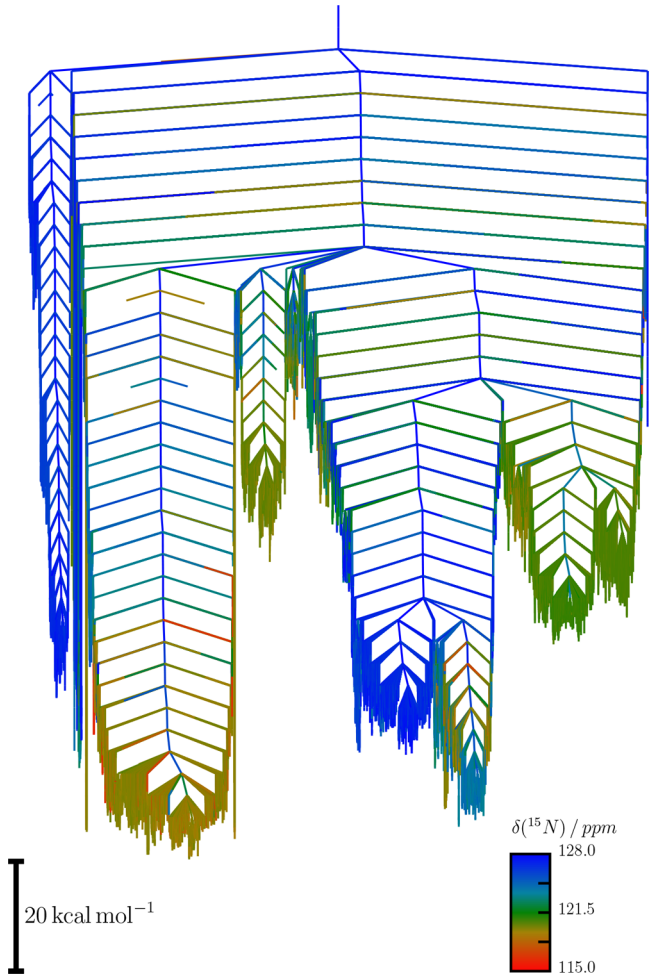

Figure 11. Potential energy disconnectivity graph for the pentamer colored using the predicted NMR shift for residue F20 of the even end strand. The difference between the entropically trapped and the canonical structures is around 3 ppm. For the structures trapped by misalignment the shift is around 5 ppm lower than for the canonical stack.

Figure 12). We are therefore able to associate the alternative traps with characteristic NMR signatures, which could potentially be observed in experiments.

The frustrated multifunnel landscape implies that the probability of observing the described subpopulations in experiments is unlikely to correspond to equilibrium but will probably be determined by kinetics. Kinetic control of the aggregation process may permit observation of subpopulations by NMR, since we predict they will be locally stable on relatively long time scales. Other techniques used to probe aggregation mechanisms, such as infrared nanospectroscopy,[106] multidimensional super-resolution imaging,[107] and cryoEM image reconstruction techniques,[108] may also be applicable.

CONCLUSIONS

The key contribution of this study is the detailed description of kinetic traps in a well-defined region of the potential and free energy landscapes for an amyloid-β pentameric stack. The main consequence of the large number of kinetic traps is a longer lifetime for misaligned structures and a significant heterogeneity in the observed conformations. Our results agree well with a number of previous studies,[28,34,36,37,44,45] particularly regarding

DOI: 10.1021/jacs.7b12896
J. Am. Chem. Soc. 2018, 140, 4018−4027

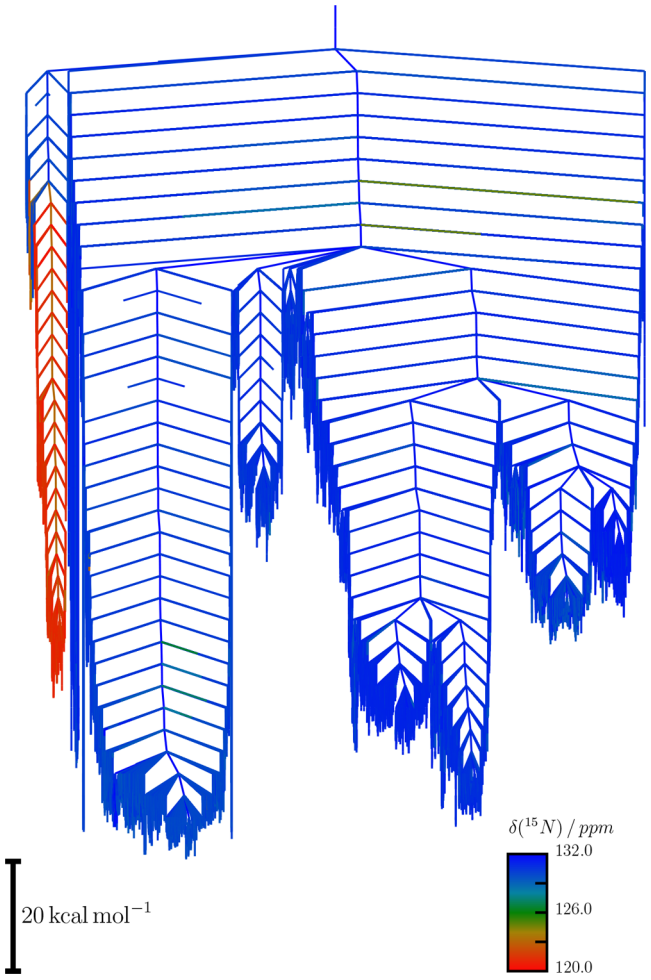

Figure 12. Potential energy disconnectivity graph for the pentamer colored using the predicted NMR shift for residue A42 of the odd end strand. The difference between the out-of-register trap and the rest of the landscape is around 12 ppm.

the series of events encountered in the aggregation process, and we suggest explanations for some of the inconsistencies previously encountered, in particular with reference to the effects of biasing forces, in agreement with other reports.[45,56]

The aggregation process for amyloid-β seems to depend on the recognition of strong interactions along the spine of the stack, and the avoidance of misalignments. Another important result is that high-entropy structures are common, in particular at the even end. Calculations need to account for this effect, and biased potentials and constraints might obscure some of these details. The changes that lead to kinetically trapped structures can be related to distinct NMR signatures.

Our study focuses on a selected region of the energy landscape based on the work by Lührs et al.[71] We plan to repeat these calculations for more recent fibril structures,[16−20] as well as regions of the landscape between the two regimes. The present results provide insight into various alternative structural models. First of all, the calculated energy barriers between morphologies are large, suggesting slow dynamics beyond the experimental observation time scale. Second, the influence of entropy and strain has systematic effects for different structural ensembles. Finally, the kinetic traps with an enthalpic origin result from misalignment of key interactions. As this effect is purely based on the initial encounter of a relatively disordered monomer with the fibril, it may be a common feature of fibril formation in other systems. Our results agree well with the work by Bacci et al.,[45] especially relating to the increased disorder of the fibril ends, which we observe using complementary methodology.

From the atomistic picture we present here, it seems unlikely that aggregation is efficient, as the multifunnel nature of the landscape produces slow time scales. As observed in experiment, this picture indicates that secondary nucleation processes are likely to be important,[9,10,44] and other surfaces or molecules may assist the aggregation process.[109]

■ ASSOCIATED CONTENT

Supporting Information

The Supporting Information is available free of charge on the ACS Publications website at DOI: 10.1021/jacs.7b12896.

Protocol for MD simulations, plots of RMSD profiles for the MD trajectories for important structures; an introductory guide to disconnectivity graphs; disconnectivity graphs with secondary structure assignments; disconnectivity graph with structures for local samples of the tetrameric landscape; predicted NMR shifts for backbone H and N for all residues for pentamer and monomer; additional disconnectivity graphs indicating the characteristic signatures of the kinetic traps (PDF)

■ AUTHOR INFORMATION

Corresponding Authors

*E-mail: kr366@cam.ac.uk.
*E-mail: dw34@cam.ac.uk.

ORCID

Konstantin Röder: 0000-0003-2021-9504
David J. Wales: 0000-0002-3555-6645

Notes

The authors declare no competing financial interest.
The research data for this article may be accessed at DOI: 10.5281/zenodo.1088750.

■ ACKNOWLEDGMENTS

We thank Prof. Birgit Strodel and Dr. Priyanka Joshi for helpful discussions and comments on the original draft. We gratefully acknowledge funding from the EPSRC.

■ REFERENCES

(1) Glenner, G. G.; Wong, C. W. *Biochem. Biophys. Res. Commun.* **1984**, *122*, 1131−1135.
(2) Masters, C. L.; Simms, G.; Weinman, N. A.; Multhaup, G.; McDonald, B. L.; Beyreuther, K. *Proc. Natl. Acad. Sci. U. S. A.* **1985**, *82*, 4245−4249.
(3) Selkoe, D. J. *Science* **2002**, *298*, 789−791.
(4) Chiti, F.; Dobson, C. M. *Annu. Rev. Biochem.* **2006**, *75*, 333−366.
(5) Nasica-Labouze, J.; Nguyen, P. H.; Sterpone, F.; Berthoumieu, O.; Buchete, N.-V.; Coté, S.; De Simone, A.; Doig, A. J.; Faller, P.; Garcia, A.; Laio, A.; Li, M. S.; Melchionna, S.; Mousseau, N.; Mu, Y.; Paravastu, A.; Pasquali, S.; Rosenman, D. J.; Strodel, B.; Tarus, B.; Viles, J. H.; Zhang, T.; Wang, C.; Derreumaux, P. *Chem. Rev.* **2015**, *115*, 3518−3563.
(6) Nagel-Steger, L.; Owen, M. C.; Strodel, B. *ChemBioChem* **2016**, *17*, 657−676.
(7) Cohen, S. I.; Vendruscolo, M.; Dobson, C. M.; Knowles, T. P. *J. Mol. Biol.* **2012**, *421*, 160−171.
(8) Arosio, P.; Knowles, T. P. J.; Linse, S. *Phys. Chem. Chem. Phys.* **2015**, *17*, 7606−7618.

DOI: 10.1021/jacs.7b12896
J. Am. Chem. Soc. 2018, 140, 4018−4027

(9) Cohen, S. I. A.; Linse, S.; Luheshi, L. M.; Hellstrand, E.; White, D. A.; Rajah, L.; Otzen, D. E.; Vendruscolo, M.; Dobson, C. M.; Knowles, T. P. J. *Proc. Natl. Acad. Sci. U. S. A.* **2013**, *110*, 9758−9763.
(10) Meisl, G.; Yang, X.; Hellstrand, E.; Frohm, B.; Kirkegaard, J. B.; Cohen, S. I. A.; Dobson, C. M.; Linse, S.; Knowles, T. P. J. *Proc. Natl. Acad. Sci. U. S. A.* **2014**, *111*, 9384−9389.
(11) Barghorn, S.; Nimmrich, V.; Striebinger, A.; Krantz, C.; Keller, P.; Janson, B.; Bahr, M.; Schmidt, M.; Bitner, R. S.; Harlan, J.; Barlow, E.; Ebert, U.; Hillen, H. *J. Neurochem.* **2005**, *95*, 834−847.
(12) Chimon, S.; Shaibat, M. A.; Jones, C. R.; Calero, D. C.; Aizezi, B.; Ishii, Y. *Nat. Struct. Mol. Biol.* **2007**, *14*, 1157−1164.
(13) Sandberg, A.; Luheshi, L. M.; Sollvander, S.; Pereira de Barros, T.; Macao, B.; Knowles, T. P. J.; Biverstal, H.; Lendel, C.; Ekholm-Petterson, F.; Dubnovitsky, A.; Lannfelt, L.; Dobson, C. M.; Hard, T. *Proc. Natl. Acad. Sci. U. S. A.* **2010**, *107*, 15595−15600.
(14) Matsumura, S.; Shinoda, K.; Yamada, M.; Yokojima, S.; Inoue, M.; Ohnishi, T.; Shimada, T.; Kikuchi, K.; Masui, D.; Hashimoto, S.; Sato, M.; Ito, A.; Akioka, M.; Takagi, S.; Nakamura, Y.; Nemoto, K.; Hasegawa, Y.; Takamoto, H.; Inoue, H.; Nakamura, S.; Nabeshima, Y.-i.; Teplow, D. B.; Kinjo, M.; Hoshi, M. *J. Biol. Chem.* **2011**, *286*, 11555−11562.
(15) Nelson, R.; Sawaya, M. R.; Balbirnie, M.; Madsen, A. Ø.; Riekel, C.; Grothe, R.; Eisenberg, D. *Nature* **2005**, *435*, 773−778.
(16) Xiao, Y.; Ma, B.; McElheny, D.; Parthasarathy, S.; Long, F.; Hoshi, M.; Nussinov, R.; Ishii, Y. *Nat. Struct. Mol. Biol.* **2015**, *22*, 499−505.
(17) Wälti, M. A.; Ravotti, F.; Arai, H.; Glabe, C. G.; Wall, J. S.; Böckmann, A.; Güntert, P.; Meier, B. H.; Riek, R. *Proc. Natl. Acad. Sci. U. S. A.* **2016**, *113*, E4976−E4984.
(18) Eisenberg, D. S.; Sawaya, M. R. *Proc. Natl. Acad. Sci. U. S. A.* **2016**, *113*, 9398−9400.
(19) Colvin, M. T.; Silvers, R.; Ni, Q. Z.; Can, T. V.; Sergeyev, I.; Rosay, M.; Donovan, K. J.; Michael, B.; Wall, J.; Linse, S.; Griffin, R. G. *J. Am. Chem. Soc.* **2016**, *138*, 9663−9674.
(20) Gremer, L.; Schölzel, D.; Schenk, C.; Reinartz, E.; Labahn, J.; Ravelli, R. B. G.; Tusche, M.; Lopez-Iglesias, C.; Hoyer, W.; Heise, H.; Willbold, D.; Schröder, G. F. *Science* **2017**, *358*, 116−119.
(21) Esler, W. P.; Stimson, E. R.; Jennings, J. M.; Vinters, H. V.; Ghilardi, J. R.; Lee, J. P.; Mantyh, P. W.; Maggio, J. E. *Biochemistry* **2000**, *39*, 6288−6295.
(22) Cannon, M. J.; Williams, A. D.; Wetzel, R.; Myszka, D. G. *Anal. Biochem.* **2004**, *328*, 67−75.
(23) Watanabe-Nakayama, T.; Ono, K.; Itami, M.; Takahashi, R.; Teplow, D. B.; Yamada, M. *Proc. Natl. Acad. Sci. U. S. A.* **2016**, *113*, 5835−5840.
(24) Klimov, D. K.; Thirumalai, D. *Structure* **2003**, *11*, 295−307.
(25) Wu, C.; Lei, H.; Duan, Y. *J. Am. Chem. Soc.* **2005**, *127*, 13530−13537.
(26) Strodel, B.; Whittleston, C. S.; Wales, D. J. *J. Am. Chem. Soc.* **2007**, *129*, 16005−16014.
(27) Nguyen, P. H.; Li, M. S.; Stock, G.; Straub, J. E.; Thirumalai, D. *Proc. Natl. Acad. Sci. U. S. A.* **2007**, *104*, 111−116.
(28) Buchete, N.-V.; Hummer, G. *Biophys. J.* **2007**, *92*, 3032−3039.
(29) Krone, M. G.; Hua, L.; Soto, P.; Zhou, R.; Berne, B. J.; Shea, J.-E. *J. Am. Chem. Soc.* **2008**, *130*, 11066−11072.
(30) Reddy, G.; Straub, J. E.; Thirumalai, D. *Proc. Natl. Acad. Sci. U. S. A.* **2009**, *106*, 11948−11953.
(31) O'Brien, E. P.; Okamoto, Y.; Straub, J. E.; Brooks, B. R.; Thirumalai, D. *J. Phys. Chem. B* **2009**, *113*, 14421−14430.
(32) Masman, M. F.; Eisel, U. L. M.; Csizmadia, I. G.; Penke, B.; Enriz, R. D.; Marrink, S. J.; Luiten, P. G. M. *J. Phys. Chem. B* **2009**, *113*, 11710−11719.
(33) Takeda, T.; Klimov, D. K. *Biophys. J.* **2009**, *96*, 4428−4437.
(34) Han, M.; Hansmann, U. H. E. *J. Chem. Phys.* **2011**, *135*, 065101.
(35) Schor, M.; Vreede, J.; Bolhuis, P. *Biophys. J.* **2012**, *103*, 1296−1304.
(36) Han, W.; Schulten, K. *J. Am. Chem. Soc.* **2014**, *136*, 12450−12460.
(37) Gurry, T.; Stultz, C. M. *Biochemistry* **2014**, *53*, 6981−6991.
(38) Schwierz, N.; Frost, C. V.; Geissler, P. L.; Zacharias, M. *J. Am. Chem. Soc.* **2016**, *138*, 527−539.
(39) Rojas, A.; Maisuradze, N.; Kachlishvili, K.; Scheraga, H. A.; Maisuradze, G. G. *ACS Chem. Neurosci.* **2017**, *8*, 201−209.
(40) Rodriguez, R. A.; Chen, L. Y.; Plascencia-Villa, G.; Perry, G. *Biochem. Biophys. Res. Commun.* **2017**, *487*, 444−449.
(41) Ban, T.; Hoshino, M.; Takahashi, S.; Hamada, D.; Hasegawa, K.; Naiki, H.; Goto, Y. *J. Mol. Biol.* **2004**, *344*, 757−767.
(42) Kellermayer, M. S. Z.; Karsai, A.; Benke, M.; Soos, K.; Penke, B. *Proc. Natl. Acad. Sci. U. S. A.* **2008**, *105*, 141−144.
(43) Qiang, W.; Kelley, K.; Tycko, R. *J. Am. Chem. Soc.* **2013**, *135*, 6860−6871.
(44) Schwierz, N.; Frost, C. V.; Geissler, P. L.; Zacharias, M. *J. Phys. Chem. B* **2017**, *121*, 671−682.
(45) Bacci, M.; Vymětal, J.; Mihajlovic, M.; Caflisch, A.; Vitalis, A. *J. Chem. Theory Comput.* **2017**, *13*, 5117−5130.
(46) Okumura, H.; Itoh, S. G. *Sci. Rep.* **2016**, *6*, 38422.
(47) Barz, B.; Strodel, B. *Chem. - Eur. J.* **2016**, *22*, 8768−8772.
(48) Bernstein, S. L.; Dupuis, N. F.; Lazo, N. D.; Wyttenbach, T.; Condron, M. M.; Bitan, G.; Teplow, D. B.; Shea, J.-E.; Ruotolo, B. T.; Robinson, C. V.; Bowers, M. T. *Nat. Chem.* **2009**, *1*, 326−331.
(49) Kawahara, M. *Curr. Pharm. Des.* **2010**, *16*, 2779−2789.
(50) Sivanesan, S.; Tan, A.; Rajadas, J. *Curr. Alzheimer Res.* **2013**, *10*, 316−323.
(51) Wang, Z.-C.; Zhao, J.; Li, S. *Neurosci. Bull.* **2013**, *29*, 752−760.
(52) Zhang, S.; Iwata, K.; Lachenmann, M.; Peng, J.; Li, S.; Stimson, E.; Lu, Y.-a.; Felix, A.; Maggio, J.; Lee, J. *J. Struct. Biol.* **2000**, *130*, 130−141.
(53) Onuchic, J. N.; Luthey-Schulten, Z.; Wolynes, P. G. *Annu. Rev. Phys. Chem.* **1997**, *48*, 545−600.
(54) Onuchic, J. N.; Wolynes, P. G. *Curr. Opin. Struct. Biol.* **2004**, *14*, 70−75.
(55) Chebaro, Y.; Ballard, A. J.; Chakraborty, D.; Wales, D. J. *Sci. Rep.* **2015**, *5*, 10386.
(56) Zheng, W.; Tsai, M.-Y.; Wolynes, P. G. *J. Am. Chem. Soc.* **2017**, *139*, 16666−16676.
(57) Weiner, S. J.; Kollman, P. A.; Nguyen, D. T.; Case, D. A. *J. Comput. Chem.* **1986**, *7*, 230−252.
(58) Pearlman, D. A.; Case, D. A.; Caldwell, J. W.; Ross, W. S.; Cheatham, T. E., III; DeBolt, S.; Ferguson, D.; Seibel, G.; Kollman, P. *Comput. Phys. Commun.* **1995**, *91*, 1−41.
(59) Case, D.; Darden, T.; Cheatham, T., III; Simmerling, C.; Wang, J.; Duke, R.; Luo, R.; Walker, R.; Zhang, W.; Merz, K.; Roberts, B.; Hayik, S.; Roitberg, A.; Seabra, G.; Swails, J.; Götz, A.; Kolossváry, I.; Wong, K.; Paesani, F.; Vanicek, J.; Wolf, R.; Liu, J.; Wu, X.; Brozell, S.; Steinbrecher, T.; Gohlke, H.; Cai, Q.; Ye, X.; Wang, J.; Hsieh, M.-J.; Cui, G.; Roe, D.; Mathews, D.; Seetin, M.; Salomon-Ferrer, R.; Sagui, C.; Babin, V.; Luchko, T.; Gusarov, S.; Kovalenko, A.; Kollman, P. *AMBER12*; University of California: San Francisco, CA, 2012.
(60) Maier, J. A.; Martinez, C.; Kasavajhala, L.; Wickstrom, L.; Hauser, K. E.; Simmerling, C. *J. Chem. Theory Comput.* **2015**, *11*, 3696−3713.
(61) Małolepsza, E.; Strodel, B.; Khalili, M.; Trygubenko, S.; Fejer, S. N.; Wales, D. J. *J. Comput. Chem.* **2010**, *31*, 1402−1409.
(62) Małolepsza, E.; Strodel, B.; Khalili, M.; Trygubenko, S.; Fejer, S. N.; Carr, J. M.; Wales, D. J. *J. Comput. Chem.* **2012**, *33*, 2209.
(63) Hornak, V.; Abel, R.; Okur, A.; Strockbine, B.; Roitberg, A.; Simmerling, C. *Proteins: Struct., Funct., Genet.* **2006**, *65*, 712−725.
(64) Onufriev, A.; Bashford, D.; Case, D. A. *J. Phys. Chem. B* **2000**, *104*, 3712−3720.
(65) Onufriev, A.; Bashford, D.; Case, D. A. *Proteins: Struct., Funct., Genet.* **2004**, *55*, 383−394.
(66) Srinivasan, J.; Trevathan, M. W.; Beroza, P.; Case, D. A. *Theor. Chem. Acc.* **1999**, *101*, 426−434.
(67) Wales, D. J.; Doye, J. P. K. *J. Phys. Chem. A* **1997**, *101*, 5111−5116.
(68) Li, Z.; Scheraga, H. A. *Proc. Natl. Acad. Sci. U. S. A.* **1987**, *84*, 6611−6615.

DOI: 10.1021/jacs.7b12896
J. Am. Chem. Soc. 2018, 140, 4018−4027

(69) Li, Z.; Scheraga, H. A. *J. Mol. Struct.: THEOCHEM* **1988**, *179*, 333.
(70) Wales, D. J. *GMIN: A program for finding global minima and calculating thermodynamic properties*; University of Cambridge: Cambridge, U.K., 2018.
(71) Lührs, T.; Ritter, C.; Adrian, M.; Riek-Loher, D.; Bohrmann, B.; Döbeli, H.; Schubert, D.; Riek, R. *Proc. Natl. Acad. Sci. U. S. A.* **2005**, *102*, 17342−7.
(72) Ryckaert, J. P.; Ciccotti, G.; Berendsen, H. J. C. *J. Comput. Phys.* **1977**, *23*, 327−341.
(73) Loncharich, R. J.; Brooks, B. R.; Pastor, R. W. *Biopolymers* **1992**, *32*, 523−535.
(74) Wales, D. J. *OPTIM - a program for optimising geometries and calculating reaction pathways*; University of Cambridge: Cambridge, U.K., 2018.
(75) *PyMOL Molecular Graphics System*, version 1.6.x; Schrödinger, L.L.C.: Cambridge, MA, 2013.
(76) Wales, D. J. *Mol. Phys.* **2002**, *100*, 3285−3305.
(77) Wales, D. J. *Mol. Phys.* **2004**, *102*, 891−908.
(78) Noé, F.; Fischer, S. *Curr. Opin. Struct. Biol.* **2008**, *18*, 154−162.
(79) Wales, D. J. *Curr. Opin. Struct. Biol.* **2010**, *20*, 3−10.
(80) Trygubenko, S. A.; Wales, D. J. *J. Chem. Phys.* **2004**, *120*, 2082−2094.
(81) Henkelman, G.; Jónsson, H. *J. Chem. Phys.* **1999**, *111*, 7010−7022.
(82) Henkelman, G.; Uberuaga, B. P.; Jónsson, H. *J. Chem. Phys.* **2000**, *113*, 9901−9904.
(83) Munro, L. J.; Wales, D. J. *Phys. Rev. B: Condens. Matter Mater. Phys.* **1999**, *59*, 3969−3980.
(84) Nocedal, J. *Math. Comput.* **1980**, *35*, 773.
(85) Liu, D.; Nocedal, J. *Math. Prog.* **1989**, *45*, 503.
(86) Götz, A. W.; Williamson, M. J.; Xu, D.; Poole, D.; Le Grand, S.; Walker, R. C. *J. Chem. Theory Comput.* **2012**, *8*, 1542−1555.
(87) Salomon-Ferrer, R.; Götz, A. W.; Poole, D.; Le Grand, S.; Walker, R. C. *J. Chem. Theory Comput.* **2013**, *9*, 3878−3888.
(88) Mantell, R. G.; Pitt, C. E.; Wales, D. J. *J. Chem. Theory Comput.* **2016**, *12*, 6182−6191.
(89) Carr, J. M.; Wales, D. J. *J. Chem. Phys.* **2005**, *123*, 234901.
(90) Wales, D. J. *PATHSAMPLE: A driver for OPTIM to create stationary point databases using discrete path sampling and perform kinetic analysis*; University of Cambridge: Cambridge, U.K., 2018.
(91) Joseph, J. A.; Röder, K.; Chakraborty, D.; Mantell, R. G.; Wales, D. J. *Chem. Commun.* **2017**, *53*, 6974−6988.
(92) Chakraborty, D.; Wales, D. J. *J. Phys. Chem. Lett.* **2018**, *9*, 229−241.
(93) Becker, O. M.; Karplus, M. *J. Chem. Phys.* **1997**, *106*, 1495−1517.
(94) Wales, D. J.; Miller, M. A.; Walsh, T. R. *Nature* **1998**, *394*, 758−760.
(95) Han, B.; Liu, Y.; Ginzinger, S. W.; Wishart, D. S. *J. Biomol. NMR* **2011**, *50*, 43−57.
(96) Kabsch, W.; Sander, C. *Biopolymers* **1983**, *22*, 2577−2637.
(97) Vitalis, A.; Caflisch, A. *J. Mol. Biol.* **2010**, *403*, 148−165.
(98) Sgourakis, N. G.; Merced-Serrano, M.; Boutsidis, C.; Drineas, P.; Du, Z.; Wang, C.; Garcia, A. E. *J. Mol. Biol.* **2011**, *405*, 570−583.
(99) Rosenman, D. J.; Connors, C. R.; Chen, W.; Wang, C.; García, A. E. *J. Mol. Biol.* **2013**, *425*, 3338−3359.
(100) Rosenman, D. J.; Wang, C.; García, A. E. *J. Phys. Chem. B* **2016**, *120*, 259−277.
(101) Petkova, A. T.; Yau, W.-M.; Tycko, R. *Biochemistry* **2006**, *45*, 498−512.
(102) Hoyer, W.; Grönwall, C.; Jonsson, A.; Ståhl, S.; Härd, T. *Proc. Natl. Acad. Sci. U. S. A.* **2008**, *105*, 5099−104.
(103) Ahmed, M.; Davis, J.; Aucoin, D.; Sato, T.; Ahuja, S.; Aimoto, S.; Elliott, J. I.; Van Nostrand, W. E.; Smith, S. O. *Nat. Struct. Mol. Biol.* **2010**, *17*, 561−567.
(104) Strodel, B.; Wales, D. J. *Chem. Phys. Lett.* **2008**, *466*, 105−115.
(105) Carr, J. M.; Wales, D. J. *J. Phys. Chem. B* **2008**, *112*, 8760−8769.
(106) Ruggeri, F. S.; Longo, G.; Faggiano, S.; Lipiec, E.; Pastore, A.; Dietler, G. *Nat. Commun.* **2015**, *6*, 7831.
(107) Bongiovanni, M. N.; Godet, J.; Horrocks, M. H.; Tosatto, L.; Carr, A. R.; Wirthensohn, D. C.; Ranasinghe, R. T.; Lee, J.-E.; Ponjavic, A.; Fritz, J. V.; Dobson, C. M.; Klenerman, D.; Lee, S. F. *Nat. Commun.* **2016**, *7*, 13544.
(108) Chen, S. W.; Drakulic, S.; Deas, E.; Ouberai, M.; Aprile, F. A.; Arranz, R.; Ness, S.; Roodveldt, C.; Guilliams, T.; De-Genst, E. J.; Klenerman, D.; Wood, N. W.; Knowles, T. P. J.; Alfonso, C.; Rivas, G.; Abramov, A. Y.; Valpuesta, J. M.; Dobson, C. M.; Cremades, N. *Proc. Natl. Acad. Sci. U. S. A.* **2015**, *112*, E1994−2003.
(109) Kedia, N.; Almisry, M.; Bieschke, J. *Phys. Chem. Chem. Phys.* **2017**, *19*, 18036−18046.

DOI: 10.1021/jacs.7b12896
J. Am. Chem. Soc. 2018, 140, 4018−4027